International Journal of Biological Macromolecules 44 (2009) 393–399

Contents lists available at ScienceDirect

International Journal of Biological Macromolecules

journal homepage: www.elsevier.com/locate/ijbiomac

Insights into the structure of the PmrD protein with molecular dynamics simulations

Vasileios A. Tatsis[a], Ioannis G. Tsoulos[b], Christos S. Krinas[a], Charalampos Alexopoulos[c], Athanassios Stavrakoudis[d,*]

[a] Department of Information and Telecommunications Engineering, University of West Macedonia, Kozani, Greece
[b] Department of Communications, Informatics and Management, Technological Educational Institute of Epirus, Arta, Greece
[c] General Chemical State Laboratory, Tsoha 16, 115 21 Athens, Greece
[d] Department of Economics, University of Ioannina, Panepistimioupoli, GR-451 10 Ioannina, Greece

ARTICLE INFO

Article history:
Received 29 December 2008
Received in revised form 24 February 2009
Accepted 25 February 2009
Available online 9 March 2009

Keywords:
β-Barrel
Computer simulation
Leucine-rich hydrophobic cluster
Molecular dynamics
Polymyxin resistance
PmrD

ABSTRACT

Resistance to cationic antimicrobial peptide polymyxin B from Gram-negative bacteria is accomplished by two-component systems (TCSs), protein complexes PmrA/PmrB and PhoP/PhoQ. PmrD is the first protein identified to mediate the connectivity between two TCSs. The 3D structure of PmrD has been recently solved by NMR and its unique fold was revealed. Here, a molecular dynamics study is presented started from the NMR structure. Numerous hydrophobic and electrostatic interactions were identified to contribute to PmrD's 3D stability. Moreover, the mobility of the five loops that connect the protein's six β-strands has been explored. Solvent-accessible surface area calculation revealed that a Leucine-rich hydrophobic cluster of the protein stabilized the protein's structure.

1. Introduction

Two separate two-component regulatory systems (TCRs), PmrA–PmrB and PhoP–PhoQ are known to be involved in the resistance to the peptide antibiotic polymyxin B and to several antimicrobial proteins from human neutrophils [1–3]. Transcription of PmrA-activated genes is promoted by either of two pathways: (i) growth in low extracellular magnesium in a process that requires PhoP–PhoQ, the second two-component regulatory system [4] and (ii) growth in the presence of high iron or acidic pH. In low Mg^{2+} concentration, PhoQ promotes phosphorylation of PhoP and transcription of PmrD. The PmrD protein binds to the phosphorylated form of PmrA, protecting it from dephosphorylation by PmrB [5].

Recently the solution NMR structure of the PmrD protein from *Escherichia coli* has been reported [6]. PmrD protein shows no homology similarity with other proteins and its three-dimensional structure is also unique. NMR studies revealed that the structure of the *E. coli* PmrD protein is consisted by six β-strands arranged in an anti-parallel β-barrel with topology 6–3–2–1–4–5–6. The C-terminal part of the polypeptide chain forms an α-helix aligned parallel to the β-barrel. The primary sequence of the *E. coli* PmrD protein shows significant similarity with PmrD proteins from other species, so it is expected that PmrD proteins share a similar fold.

The secondary structure of PmrD is consisted by six β-strands forming an anti-parallel β-barrel (6–3–2–1–4–5–6 topology) and a C-terminal α-helix [6]. Comparison with other proteins structures with DALI server did not revealed any significant similarity with other protein folds. PmrD is also characterized by a well-formed Leucine-rich hydrophobic cluster that probably stabilizes its tertiary structure. Thus, it is very interesting to see about the stability of these structures as revealed by molecular dynamics simulations. In this work we present a molecular dynamics study of PmrD protein in aqueous solution starting from the NMR solved structure. This aims at providing a high-resolution atomistic view of specific interactions that cannot be easily captured by experimental techniques [7] which suffer from space or/and time averages [8]. Such type of complementary investigations have been proved to enlighten our knowledge of peptides/proteins structural properties and to help in better understanding of their action [9]. Recent simulation studies have enlighten our understanding of non-bonded interactions that stabilize secondary peptide structures [10] or promote folding [11]. One of the main targets of this study was to explore the five loop dynamics that connect the six strands region

* Corresponding author. Tel.: +30 265 109 5935; fax: +30 265 109 5092.
E-mail address: astavrak@cc.uoi.gr (A. Stavrakoudis).
URL: http://stavrakoudis.econ.uoi.gr/ (A. Stavrakoudis).

0141-8130/$ – see front matter © 2009 Elsevier B.V. All rights reserved.
doi:10.1016/j.ijbiomac.2009.02.006

of PmrD's β-barrel structure. It is well known that loop region on the surface of the protein structure play important role in protein recognition phenomena. Thus a detailed picture of the dynamics of these regions might help our understating of the role of PmrD protein. Another important target was to investigate the electrostatic interactions found on the surface on the protein.

2. Computational methods

Initial protein coordinates were extracted from *E. coli* PmrD NMR structure as deposited at PDB, access code 2JSO [6]. Starting conformation was build from the first model of NMR derived bundle of structures using the VMD program [12]. As it has been shown recently, MD results do not differ significantly if a different structure from the NMR bundle is used [10]. The protein was solvated with 9935 TIP3P [13] water molecules using a rectangular box with dimensions 6.33 nm × 7.20 nm × 7.32 nm. This allowed a distance of at least 1.8 nm between any peptide atom and the edges of the box in order to avoid simulation artifacts [14]. The system was neutralized by placing 22 Na^+ and 25 Cl^- ions using VMD's solvate and autoionize plugins. From this point on, all subsequent MM and MD runs were performed with the NAMD program (v2.6) [15] using 12 CPUs of a Linux cluster. Topology and force field parameters for all atoms were assigned from the CHARMM27 parameter set [16]. Non-bonded van der Waals interactions were gradually turned off at a distance between 1.0 and 1.2 nm. The non-bonded pair list was updated every 10 steps. Long range electrostatics were computed at every step with the PME [17] method, with a grid spacing of less than 0.1 nm. Bonds to hydrogen atoms were constrained with the SHAKE [18] with a relative tolerance of 10^{-8}, allowing a 2 fs step during subsequent MD runs. The whole system, consisted by 15,591 atoms, was energy minimized with 2000 steps of conjugate gradients. After minimization the temperature of the system was gradually increased with Langevin dynamics, using the NVT ensemble, to 298 K, during a period 3000 steps, by stepwise reassignment of velocities every 500 steps. At this stage, heavy atoms of the peptide model were restrained to their initial positions with a force constant of 50 kcal mol^{-1} Å^{-2}. The simulation continued until 100,000 steps (0.2 ns). The force constant of positional restraints was then decreased to 5 kcal mol^{-1} Å^{-2} for another 100,000 steps and finally positional restraints were totally eliminated for subsequent 200,000 steps of NVT equilibration period. The simulation was continued under constant pressure, with Langevin piston method [19], thus NPT ensemble, for 40 ns. Pressure was maintained at 1 atm and temperature was kept at 298 K. The results presented here are from this, isothermal–isobaric ensemble, MD run. Snapshots were saved to disk at 1 ps interval for further analysis.

Conformation analysis and visual inspection of structures were performed with VMD [12], Carma [20] and Eucb [21] software packages. Secondary structure assignment was performed with STRIDE [22]. Structural figures were prepared with PYMOL [23].

Root mean square calculations have been performed after removal of the global rotation/translation of the trajectory frames by fitting all the protein atoms to the conformation of the first frame.

The root mean square distance (RMSD) between the backbone atoms of the trajectory frames of polypeptide chains and the corresponding atoms of the NMR structure, calculated for frame t, is given by Eq. (1), where x^m, y^m, z^m are the Cartesian coordinates found at the NMR structure and x^t, y^t, z^t are the Cartesian coordinates of trajectory frame t. N is the number of atoms:

$$\mathrm{RMSD}_t = \sqrt{\frac{1}{N}\sum_{i=1}^{N}(x_i^m - x_i^t)^2 + (y_i^m - y_i^t)^2 + (z_i^m - z_i^t)^2} \quad (1)$$

The root mean square fluctuation (RMSF) of an atom is a measure of the deviation between the position of the atom and some reference position:

$$\mathrm{RMSF} = \sqrt{\frac{1}{T}\sum_{i=1}^{T}(x_i - \bar{x})^2} \quad (2)$$

where T is the number of trajectory frames and $\bar{x}$ is the time-averaged position. Practically, RMSF calculates the mobility of an atom during the MD trajectory, thus higher RMSF values indicate higher mobility and lower RMSF values indicate restricted mobility.

Side chain hydrophobic interactions were measured as follows: for every pair of residues all the distances between the side chain heavy atoms were computed and the lower one was kept as the side chain distance. Two residues were assigned to have hydrophobic contact if this distance was found less than 0.4 nm for at least 30% of the trajectory frames (or 30% of the structures from the NMR bundle).

Hydrogen bond assignment was based on geometrical criteria: donor–acceptor distance to be less than 0.32 nm and donor–hydrogen–acceptor angle to be greater than 120°.

Salt bridges were assigned if two oppositely charged atoms were found in distance less than 0.4 nm. In cases of multiple atoms present, for example in Arg/Asp pair, the smallest distance (there are six N–O distances) was taken into consideration.

PmrD's supersecondary structure is consisted by six β-strands and one α-helix. Loops connecting the β-strands are numbered by the first strand, thus loop 1 connects strands β1 and β2, loop 2 connects strands β2 and β3, etc.

Search for β-turns was based on C$\alpha(i)$–C$\alpha(i+3)$ distance and C$\alpha(i)$–C$\alpha(i+1)$– C$\alpha(i+2)$–C$\alpha(i+3)$ dihedral angle. A β-turn was accepted if the distance was found to be less than 0.7 nm and the absolute value of the dihedral angle bigger than 90°. Backbone dihedral (φ, ψ) of the $i+1$, $i+2$ residues were used in order to define the β-turn type.

Averaged distances between H^{α} and H^{N} atoms were computed by the formula:

$$d_{ij} = \langle r_{ij}^{-1/6} \rangle^{1/6} \quad (3)$$

where r_{ij} is the Euclidean distance between atoms i and j, measured from Cartesian coordinates of trajectory frames. A table of the NOE input restraints for NMR based structure calculation and corresponding MD averaged distances is given in supplementary material.

Calculation of solvent-accessible surface area (SASA) was performed with NACCESS [24].

3. Results and discussion

3.1. RMSF and RMSD trajectory analysis

Fig. 1 shows the superimposition of representative structures obtained from MD trajectory over the starting conformation. RMSF values of C^{α} atoms are shown in Fig. 2A. With the exception of the C-terminal part the rest of the polypeptide chain shown minimal fluctuations. RMSF values below 0.1 nm were recorded for most of the residues. However, residues of the loops 1 and 2, regions 10–14 and 23–27 respectively, showed increased RMSF values close to 0.2 nm. This is somewhat expected as exposed loops in protein structures usually undergo increased flexibility. It is notable that RMSF values from NMR and MD data followed a very similar pattern. Obviously, MD produced larger RMSF values (unrestrained versus restrained dynamics) but both methods identified the same regions as the most mobile ones.

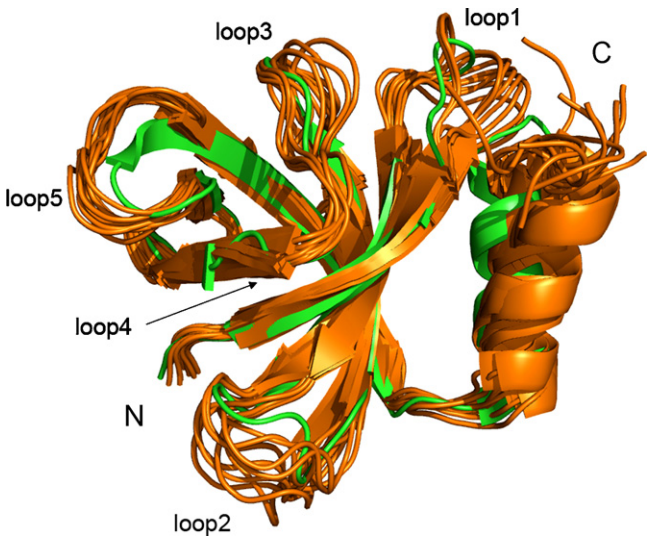

Fig. 1. Cartoon representation of 10 representative structures (every 4 ns) from MD trajectory superimposed on the starting conformation (colored green). (For interpretation of the references to color in this figure legend, the reader is referred to the web version of the article.)

Fig. 2B shows the time evolution of RMSD of backbone atoms or PmrD relatively to the initial coordinates. It is evident that the overall structure showed only moderate fluctuation with RMSD ranged between 0.2 and 0.25 nm for most of the time.

Fig. 2C shows the RMSD time evolution of the backbone of the five loops that connect the six β-strands of the PmrD protein. Loops 2–5 showed minimal fluctuations with remarkably stable RMSD time series. Loop 1 (residues 10–14) showed a small conformational transition at approximately 10–11 ns of the simulation where RMSD value changed from ~0.10 to ~0.17 nm.

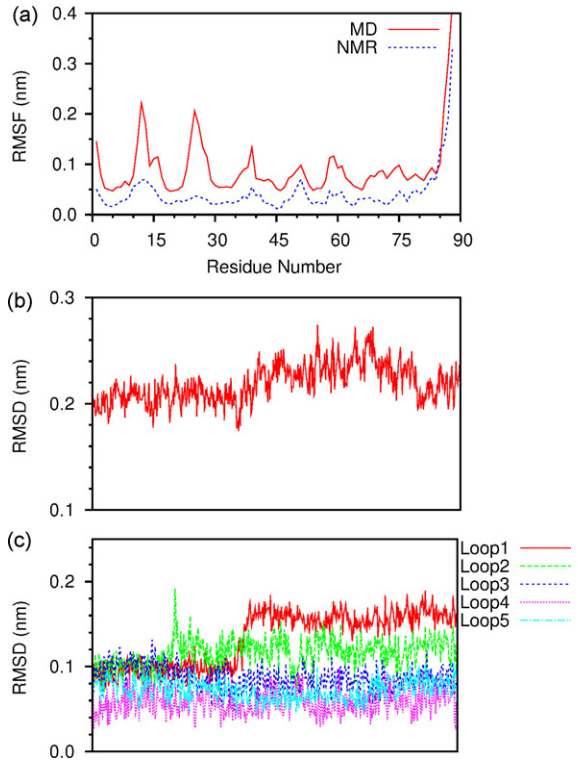

Fig. 2. Root mean square fluctuation (RMSF) of the *E. coli* PrmD residues's Cα atoms (A) and root mean square distance of the protein's heavy atoms (B). Root mean square distance of *E. coli* PrmD's loops (B). L1, . . ., L5 stands for the five corresponding loops of PrmD.

It is interesting to note that loops 1–5 showed gradually decreased conformational mobility, as it is indicated both from RMSF and RMSD plots.

In general, both RMSF and RMSD plots indicate the relative stability of the MD trajectory. As it was expected, loop residues showed increased mobility relatively to strand or helical residues, mainly due to their exposed position: there are fewer interactions in exposed loop regions than in the core of the protein 3D structure, which is consisted by the six β-strands. Good agreement between experimental and simulated structures can also be verified by comparison of the input NOE restraints and MD-averaged proton-proton distances (table supplied as supplement). Although only backbone (H^{α}, H^{N}) protons were included in the computations, the minor differences between experimental and simulated based inter-proton distances confirmed the validity of the simulated structures and the MD trajectory. This fact allowed us to proceed with further analysis.

3.2. Backbone conformation and secondary structure

Table 1 shows the percentage of the conservation of each of the secondary structure elements during the MD trajectory (a plot that shows the time evolution of STRIDE secondary structure assignment is supplied in supplement material). From our analysis it can be concluded that all main secondary structural features of PmrD were very well conserved. It has been also observed that ending residues escaped from the initial conformational state in some of the cases. For example, β2 strand of residues His_{17}-Asp_{23} was conserved for 16% of the time. This percentage was found 82% for the fragment His_{17}-Cys_{22} indicating that Asp_{23} did not retained its initial strand conformation. Overall, in line with the previously analyzed RMSD time series, only moderate fluctuations of the backbone structure were observed.

Table 1
Summary of secondary structure of the PmrD protein, during the MD study. Percentages of structure from NMR bundle of structure and MD trajectory are given.

Secondary structure	Region	NMR	MD
α-Helix	Pro_{74}-Ala_{84}	100	99
β1	Trp_{3}-Cys_{9}	100	33
β2	Arg_{16}-Cys_{22}	86	64
β3	Lys_{29}-Ser_{36}	100	42
β4	Asp_{44}-Pro_{48}	100	91
β5	Leu_{53}-Asn_{57}	100	99
β6	Glu_{59}-Ser_{71}	76	47
β-Turn	Leu_{5}-Gly_{8}	100	16
β-Turn	Asn_{11}-Asp_{14}	–	99
β-Turn	Lys_{12}-Asn_{15}	100	32
β-Turn	Asp_{23}-Gly_{26}	100	96
β-Turn	Gly_{26}-Lys_{29}	95	18
β-Turn	Ser_{36}-Ala_{39}	43	71
β-Turn	Lys_{41}-Asp_{44}	100	89
β-Turn	Pro_{48}-Asn_{51}	33	40
β-Turn	Gln_{50}-Leu_{53}	100	100
β-Turn	Cys_{55}-Arg_{58}	48	24
β-Turn	Ile_{56}-Glu_{59}	90	35
β-Turn	Lys_{60}-Thr_{63}	–	48
β-Turn	Val_{66}-Ala_{69}	–	28
β-Turn	Ser_{73}-Glu_{76}	100	78
β-Turn	Pro_{74}-Trp_{77}	100	87
β-Turn	Asp_{75}-Glu_{78}	100	96
β-Turn	Glu_{76}-Arg_{79}	100	98
β-Turn	Trp_{77}-Gln_{80}	100	94
β-Turn	Glu_{78}-Cys_{81}	100	100
β-Turn	Arg_{79}-Lys_{82}	62	92
β-Turn	Gln_{80}-Val_{83}	86	87
β-Turn	Cys_{81}-Ala_{84}	71	98
β-Turn	Lys_{82}-Gly_{85}	43	97
β-Turn	Val_{83}-Lys_{86}	100	28
β-Turn	Gly_{85}-Gln_{88}	–	42

See text for more details.

Table 2
Secondary structure assignment of the five loops of the PmrD protein in starting conformation (NMR) and during MD trajectory.

Loop	Sequence	NMR	MD	Occurrence (%)
1	Cys_{10}-Arg_{16}	CCTTTTE	CTTTTTE	25
			ETTTTCE	24
			ETTTTTE	12
2	Ala_{24}-Lys_{29}	TTTTTE	TTTCCE	42
			TTTCCC	37
			TTTTTE	12
3	Asp_{37}-Gly_{43}	TTTCTTT	TTTCTTT	64
			CCCCTTT	22
4	Leu_{49}-Ala_{52}	CTTT	CTTT	60
			TTTT	40
5	Asn_{57}-Lys_{60}	ETEE	TTTT	25
			CCCC	20
			CCCT	19

3.3. Loop dynamics

Loops and/or turn connecting strands play always important role in protein structure and function especially in protein recognition processes. Thus it is very interesting to see how the loops and turns of the PmrD protein behaved during the simulated trajectory. Table 2 summarizes the secondary structure assignment of the five loops of the PmrD protein, from both NMR and MD structures.

Residues Cys_{10}-Arg_{16} constituted the first loop connecting the β1 and β2 strands. A type IV β-turn was found in the NMR structure in the fragment Lys_{12}-Asn_{15}. This β-turn was conserved for 46% of the trajectory frames (Table 1). This β-turn was not stabilized by backbone hydrogen bond. NMR data indicated the existence of a side chain interaction between Asn_{15}:$N^{\delta 2}$ and Lys_{12}:O. This pair of atoms was found in hydrogen bond state in 12 (out of 21) structures in NMR bundle of conformers and in 88% of the trajectory frames (Table 3). Within the Cys_{10}-Arg_{16} fragment (loop 1) there was another β-turn that it appeared in the MD trajectory but not found in the initial structure. Fragment Asn_{11}-Asp_{14} formed a β-turn for 99% of the trajectory time (Table 1).

Loop 2 was constituted by residues Ala_{24}-Lys_{29}. Two β-turns were found in the NMR bundle of structures within loop 2 sequence: fragments Asp_{23}-Gly_{26} and Gly_{26}-Lys_{29} of types IV and VIII respectively. The type IV β-turn of the fragment Asp_{23}-Gly_{26} was very well conserved during the MD trajectory: 99% of the frames were satisfied the geometrical criteria for β-turn (Table 1). The characteristic $i \leftarrow i+3$ backbone hydrogen bond was detected in the MD trajectory. Anyway, side chain carboxyl group of Asp_{23} and backbone amide group of Gly_{26} were found hydrogen bonded for approximately 49% of the time (Table 3). The second β-turn (fragment Gly_{26}-Lys_{29}) was poorly conserved during MD, only ~15% of the frames retained the β-turn structure (Table 1).

Loop 3, fragment Asp_{37}-Gly_{43}, was found in TTTCTTT conformation in the NMR structure. This conformational was conserved for 75% of the simulation time (Table 2). Residues Asp_{37}-Ala_{39} lost the turn conformation for some period of the simulation time and adopted coil conformation. Thus the fragment Asp_{37}-Gly_{43}, was found in CCCCTTT for 20% of the simulation time (Table 2). In general, these results indicate the stability of the loop structure.

Loop 4, fragment Leu_{49}-Ala_{52}, was found in CTTT conformation in the NMR structure. For 55% of the trajectory frames it remained in CTTT state, while for the rest of the 45% of the trajectory frames the TTTT conformation was observed (Table 2). Asn_{51} and Ala_{52} residues were located in the central part of a type I β-turn. A backbone hydrogen bond, $Leu_{53} \leftarrow Gln_{50}$, was observed in 18 out of 21 deposited NMR structures. This hydrogen bond was conserved in 96% of the simulation time (Table 3).

Loop 5, fragment Asn_{57}-Lys_{60}, was found in ETEE conformational state in the NMR structure. As it is indicated in the Table 2, residues of this tetramer fragment adopted mostly turn-type conformation. However, the type IV β-turn in the initial structure was not perfectly conserved during MD trajectory. Only 41% of the frames (Table 1) preserved the turn conformation.

Table 3
Hydrogen bonds of the PmrD protein.

Donor	Acceptor	NMR	MD	Donor	Acceptor	NMR	MD
Trp_3:N	Leu_{46}:O	2.82	79	Ser_{36}:N	Asn_{15}:O	3.93	52
Leu_4:N	Cys_{22}:O	2.82	99	Lys_{41}:N	Asp_{44}: $O^{\delta 2}$	2.89	33
Val_5:N	Asp_{44}:O	2.90	–	Lys_{41}:N^{ζ}	Asp_{44}: $O^{\delta 1}$	2.76	53
Lys_6:N	Met_{20}:O	3.09	93	Lys_{41}:N^{ζ}	Asp_{44}: $O^{\delta 2}$	3.89	53
Lys_7:N	Met_{20}:O	3.07	–	Gly_{43}:N	Val_5:O	2.85	84
Cys_9:N	Val_{18}:O	2.90	78	Leu_{46}:N	Trp_3:O	2.82	99
Asn_{11}:$N^{\delta 2}$	Arg_{16}:O	3.23	36	Leu_{49}:N	Leu_{53}:O	2.87	52
Asn_{15}:N	Asn_{11}:$O^{\delta 1}$	3.05	–	Gln_{50}:N	Leu_{53}:O	3.33	–
Arg_{16}:N	Asp_{14}:O	3.68	36	Tyr_{54}:N	Val_{64}:O	3.00	–
Arg_{16}:N^{ε}	Asp_{14}:$O^{\delta 1}$	5.25	36	Cys_{55}:N	Ser_{47}:O	2.84	98
Arg_{16}:$N^{\eta 1}$	Glu_{33}:$O^{\varepsilon 2}$	2.77	34	Ile_{56}:N	His_{62}:O	2.82	75
Arg_{16}:$N^{\eta 2}$	Asp_{14}:$O^{\delta 2}$	2.78	30	Asn_{57}:N	Leu_{45}:O	2.93	–
His_{17}:N	Val_{34}:O	2.85	75	Asn_{57}:$N^{\delta 2}$	Asp_{44}: $O^{\delta 1}$	2.78	–
Val_{18}:N	Cys_9:O	4.04	78	Asn_{57}:$N^{\delta 2}$	Asp_{44}: $O^{\delta 2}$	4.58	24
Leu_{19}:N	Ala_{32}:O	3.02	–	Leu_{61}:N	Glu_{59}:O	3.53	35
Met_{20}:N	Lys_7:O	2.90	–	Val_{64}:N	Tyr_{54}:O	2.98	98
Leu_{21}:N	Met_{30}:O	2.99	–	Val_{66}:N	Ala_{52}:O	2.81	–
Cys_{22}:N	Leu_4:O	2.85	–	Leu_{67}:N	Glu_{33}:O	2.87	–
Asp_{23}:N	Asp_{23}: $O^{\delta 2}$	4.34	33	Ser_{70}:N	Ile_{31}:O	2.95	–
Gly_{25}:N	Asp_{23}: $O^{\delta 2}$	3.37	24	Tyr_{72}:N	Lys_{29}:O	3.40	–
Gly_{26}:N	Asp_{23}: $O^{\delta 2}$	3.23	37	Trp_{77}:N	Ser_{73}:O	2.89	52
Ala_{27}:N	Asp_{23}: $O^{\delta 2}$	2.98	57	Glu_{78}:N	Pro_{74}:O	3.01	–
Met_{30}:N	Leu_{21}:O	2.76	–	Arg_{79}:N	Asp_{75}:O	2.93	–
Ile_{31}:N	Ser_{70}:O	2.86	77	Arg_{79}:N^{ε}	Glu_{76}:$O^{\varepsilon 2}$	6.20	20
Ala_{32}:N	Leu_{19}:O	2.89	–	Arg_{79}:$N^{\eta 2}$	Glu_{76}:$O^{\varepsilon 2}$	6.58	51
Glu_{33}:N	Ser_{68}:O	2.84	91	Gln_{80}:N	Glu_{76}:O	3.16	64
Val_{34}:N	His_{17}:O	2.92	96	Cys_{81}:N	Trp_{77}:O	2.97	92
Lys_{35}:N	Lys_{65}:O	2.84	29	Lys_{82}:N^{ζ}	Glu_{78}:O	5.86	75
Lys_{35}:N^{ζ}	Asp_{37}: $O^{\delta 1}$	10.04	41	Val_{83}:N	Arg_{79}:O	3.07	–
Lys_{35}:N^{ζ}	Asp_{37}: $O^{\delta 2}$	11.98	39	Ala_{84}:N	Gln_{80}:O	3.00	77

The NMR column shows the donor–acceptor distance in the starting conformation and the percentage of structures that met the geometrical criteria for hydrogen bond. The MD column shows the percentage of frames that met the geometrical criteria for hydrogen bond.

3.4. Interactions between secondary structure elements

Several interactions were observed between the β-strands and/or the α-helical region of the PmrD protein. A figure that summarizes the important hydrogen bonds and hydrophobic interactions and depicts their network that stabilized the PmrD's tertiary structure is provided in supplement material.

Interactions between strands 6 and 3 were dominated by hydrogen bonds between Ser_{70}:N-Ile_{31}:O, Leu_{67}:N-Glu_{33}:O and Glu_{33}:N-Ser_{68}:O pairs. These three hydrogen bonds were found in >99% of the trajectory frames, in accordance with the NMR data. Moreover, MD indicated the existence of a bifurcated hydrogen bond between Glu_{33}:O and Ser_{68}:N, but only in 47% of the frames. The corresponding average distance in the NMR structure (0.33 nm) also indicated a weak hydrogen bond.

Six hydrogen bonds were found between strands 3 and 2. Four of them, His_{17}:N-Val_{34}:O, Val_{34}:N-His_{17}:O, Ala_{32}:N-Leu_{19}:O and Met_{30}:N-Leu_{21}:O, were found in 89-100% of the frames, thus in very well agreement with NMR structure. Moreover, analysis of MD trajectory revealed two additional hydrogen bonds, not existed in the NMR structure, between Leu_{21}:N-Met_{30}:O (100%) and Ser_{36}:O^{γ}-His_{17}:$N^{\delta 1}$ (48%) pairs. Hydrophobic interactions between Leu_{19}-Val_{34} and Leu_{21}-Ala_{32} side chains were retained for 93% and 83% of the trajectory.

Table 4
Hydrophobic interactions between side chains of aliphatic and/or aromatic residues.

Residue #1	Residue #2	NMR		MD	
Leu_4	Leu_{45}	0.559 (0.017)	–	0.414 (0.046)	47
Val_5	Leu_{19}	0.359 (0.006)	100	0.406 (0.026)	46
Val_5	Leu_{21}	0.540 (0.053)	–	0.395 (0.027)	63
Val_5	Val_{40}	0.421 (0.017)	–	0.414 (0.037)	40
Val_5	Leu_{46}	0.377 (0.006)	100	0.416 (0.042)	39
Val_{18}	Ile_{31}	0.378 (0.022)	86	0.414 (0.036)	47
Val_{18}	Ala_{84}	0.401 (0.023)	52	0.492 (0.148)	31
Leu_{19}	Leu_{21}	0.446 (0.068)	33	0.394 (0.025)	64
Leu_{19}	Val_{34}	0.361 (0.009)	100	0.372 (0.019)	93
Leu_{19}	Val_{40}	0.379 (0.008)	100	0.409 (0.037)	45
Leu_{19}	Leu_{46}	0.392 (0.006)	95	0.414 (0.038)	38
Leu_{21}	Ala_{32}	0.376 (0.009)	100	0.381 (0.030)	78
Leu_{21}	Leu_{46}	0.366 (0.005)	100	0.407 (0.035)	47
Val_{66}	Val_{34}	0.379 (0.031)	71	0.381 (0.030)	81
Val_{40}	Ile_{56}	0.389 (0.015)	81	0.419 (0.049)	41
Val_{64}	Leu_{46}	0.380 (0.018)	90	0.398 (0.032)	58
Val_{64}	Ile_{56}	0.382 (0.019)	71	0.381 (0.029)	76
Trp_3	Leu_{21}	0.390 (0.034)	53	0.389 (0.027)	70
Trp_3	Ile_{28}	0.550 (0.029)	–	0.448 (0.103)	44
Trp_3	Met_{30}	0.544 (0.045)	–	0.422 (0.060)	47
Trp_3	Tyr_{54}	0.431 (0.044)	24	0.427 (0.049)	32
Phe_{38}	His_{62}	0.353 (0.010)	100	0.389 (0.037)	79
Tyr_{54}	Leu_{46}	0.402 (0.009)	33	0.401 (0.027)	51
Tyr_{54}	Pro_{48}	0.390 (0.008)	91	0.419 (0.032)	31
Tyr_{54}	Val_{66}	0.369 (0.015)	100	0.372 (0.025)	87
His_{62}	Ile_{56}	0.520 (0.010)	–	0.482 (0.048)	25
Tyr_{72}	Ile_{31}	0.383 (0.010)	100	0.410 (0.037)	47
Tyr_{72}	Pro_{74}	0.432 (0.016)	–	0.436 (0.051)	24
Trp_{77}	Val_{18}	0.494 (0.088)	33	0.412 (0.053)	51
Trp_{77}	Met_{20}	0.471 (0.020)	–	0.403 (0.038)	57
Trp_{77}	Ile_{31}	0.437 (0.049)	33	0.410 (0.037)	46

Average distance (in nm), standard deviation (in parentheses) and percentage of structures (NMR bundle) or trajectory frames (MD) that the corresponding distance was found less than 0.4 nm are given.

Four hydrogen bonds were found between strands 2 and 1 during the MD trajectory. Three of them, Cys_{22}:N-Leu_4:O, Met_{20}:N-Lys_7:O and Leu_4:N-Cys_{22}:O, that existed in the NMR structure were also retained in the MD trajectory for at lest 98% of the simulation time. A fourth hydrogen bond between Val_{18}:N-Cys_9:O also appeared (96%) and contributed to the stability of the inter-strand interaction. The Val_{18}:N-Cys_9:O distance in the NMR structure was found to be around 0.38 nm, thus not to big but certainly not in hydrogen bond state. Side chain interactions between Val_5-Leu_{19}, Val_5-Leu_{21} and Trp_3-Leu_{21} residue pairs, with corresponding distances found less than 0.4 nm in 48–71% of the frames, contributed also to the inter-strand stabilization.

Three hydrogen bonds were found between residues of strands 1 and 4. Thus hydrogen bonds between Leu_{46}:N-Trp_3:O, Val_5:N-Asp_{44}:O and Trp_3:N-Leu_{46}:O existed for more than 96% of the simulation time, in very good agreement with the NMR structure. Relatively weak hydrophobic interactions between side chains of Leu_4-Leu_{45} (43%) and Val_5-Leu_{46} (36%) were also recorded.

Interactions between strands 4 and 5 were limited between Cys_{55}:N-Ser_{47}:O (100%) and Ser_{47}:N-Cys_{55}:O (100%). The second was not found in the NMR structure, where the corresponding distance is approximately 0.4 nm. Side chain hydrophobic interaction between Leu_{46} and Tyr_{54} was also observed, where the distance between the two side chains were found less than 0.4 nm for 50% of the simulation time.

Three hydrogen bonds between Val_{64}:N-Tyr_{54}:O, Tyr_{54}:N-Val_{64}:O and Lys_{35}:N-Lys_{65}:O were dominated the inter-strand interactions between strands 5 and 6. They all were found in more than 99% of the trajectory frames, in accordance with NMR structure. Hydrophobic interactions between Tyr_{54} and Val_{66} side chains, with 87% of the frame at distance less than 0.4 nm, also contributed to the stability of the inter-strand arrangement.

3.5. Dynamics of the C-terminal α-helix

The helical part of C-terminal PmrD structure remained stable during MD trajectory. Molecular dynamics simulations of isolated peptides have revealed some α- to π-helix interconversion when the CHARMM27 force field has been applied without the CMAP correction term [25,26]. Such a conformational shift was not observed within the current study.

Side chain of Trp_{77} dominated the interactions of the helical part of PmrD with the β-barrel part. This side chain was found in close contact with Val_{18}, Met_{20} and Ile_{31} (Table 4, supplement material). The first residues are from β1 strand and the third one from β2 strand. Another important interaction that was found was the salt bridge between C-terminal carboxyl group of Gln_{88} and Lys_{12} at loop 1 (Table 5).

3.6. Electrostatic interactions and salt bridges

It has been hypothesized that loops 1 and 2 are responsible for PmrA binding. Loop 1 contained Asp_{14} and Arg_{16} residues

Table 5
Salt bridges formed between charged side chains of the PmrD protein.

Positive	Negative	MD	NMR
Arg_{16}	Asp_{14}	65	100
Arg_{16}	Glu_{33}	75	100
Lys_{35}	Asp_{37}	60	–
Lys_{41}	Asp_{44}	83	95
Arg_{58}	Glu_{59}	55	20
Arg_{79}	Asp_{75}	23	69
Arg_{79}	Glu_{76}	89	69

Percentage of occurrence during MD trajectory and NMR bundle of structures are given.

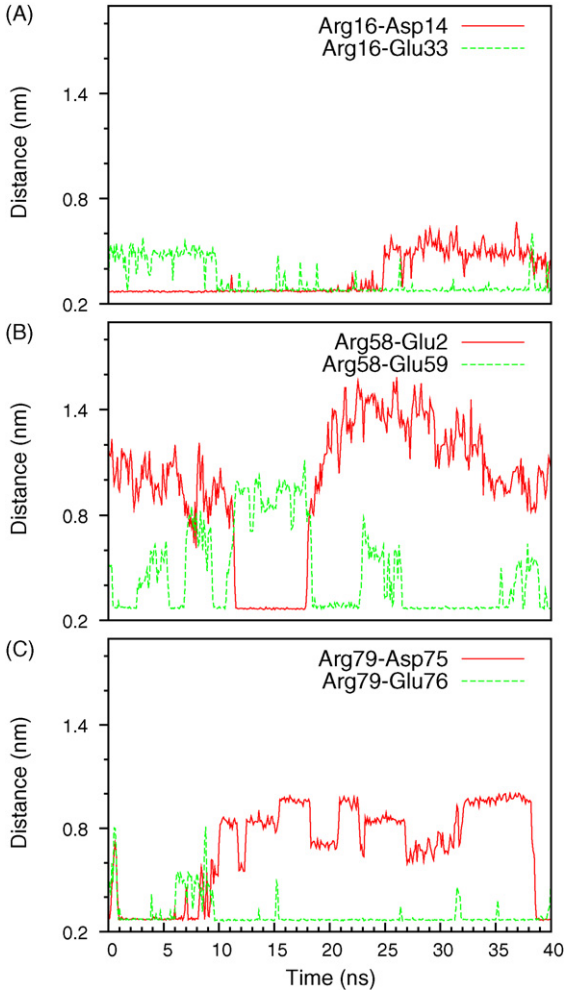

Fig. 3. Time evolution of salt bridges distances. (A) Time series of the Arg_{16}–Asp_{14} (red line), Arg_{16}-Glu_{33} (green line) distances from the MD trajectory of the protein PrmD, (B) Arg_{58}-Glu_2 (red line), Arg_{58}-Glu_{59} (green line) distances from the MD trajectory of the protein, (C) time series of the Arg_{79}-Asp_{75} (red line), Arg_{79}-Glu_{76} (green line) distances from the MD trajectory of the protein and (D) time series of the Arg_{82}-Glu_{78} (red line) and Arg_{86}-Glu_{78} (green line) distances from the MD trajectory of the protein. (For interpretation of the references to color in this figure legend, the reader is referred to the web version of the article.)

which were found to interact electrostatically via their side chains (Table 5). This interaction resembles the well-known RGD motif responsible for cell adhesion processes [27]. Side chain interactions between arginine and aspartic side chains have been studied with NMR and MD approaches [28–31] in model peptides. It has been proposed that carboxylic and guanidinium groups are directed in a synplanar orientation and that arrangement facilitates the binding process. A dihedral angle of orientation (*pdo*) has been proposed as a metric of this particular type of interaction. Thus, the dihedral between Asp_{16}:C^{γ}-Asp:C^{α}-Arg:C^{α}-Arg:C^{ζ} (*pdo*) has been measured. The *pdo* was found in the range $[-45^{\circ}, 45^{\circ}]$ for 98% of the trajectory frames (20 out of 21 models in the NMR structure). Thus, both NMR and MD simulation indicated the synplanar orientation of these side chain groups. This 3D motif might play an important role in PmrD/PmrA interactions.

A series of salt bridges were found between the oppositely charged side chains to stabilize the 3D structure of PmrD (Table 5). Interestingly, for some of the cases complex salt bridges appeared where a positive residue was found to interact with two negative residues, not necessarily at the same time. The most striking example comes from the Asp_{14}/Arg_{16}/Glu_{33} triad (Fig. 3). Arg_{16} and Asp_{14}

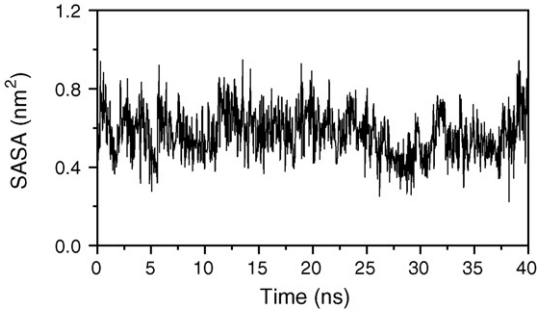

Fig. 4. Time evolution of solvent-accessible surface area (SASA) of the Leucine-rich hydrophobic cluster. Only side chain atoms were taken into consideration from residues Val_5, Leu_4, Leu_{19}, Leu_{21}, Val_{34}, Leu_{46} and Tyr_{54} are taken into consideration.

side chains remained in hydrogen bond state or salt bridge (Table 3, Table 5) during the whole trajectory. After the 10th ns of the simulation time, Glu_{33}'s side chain was also approached Arg_{16}'s side chain and a complex interaction was formed where guanidinium of Arg_{16} was simultaneously hydrogen bonded with Asp_{14}'s and Glu_{33}'s side chain carboxylic groups.

Another interesting example was the Arg_{58}/Glu_{59}/Glu_2 triad (Fig. 3). Two adjacent residues of loop 5, Arg_{58} and Glu_{59}, formed a salt bridge, something that is somewhat expected, although not very stable (Table 5). When, after the 10th ns of the simulation the interaction was broken and the distance between Arg_{58} and Glu_{59} was above 0.8 nm, Glu_2's (N-terminal, close to β1 strand) side chain approached the Arg_{58}'s side chain and a new salt bridge (hydrogen bond) was formed. At approximately the 18th ns of the simulation the situation changed again, The Arg_{58}-Glu_{59} interaction broke and the pair Arg_{58}-Glu_2 was found to interact.

3.7. Hydrophobic cluster

PmrD's 3D structure contains several hydrophobic residues that form a well-formed cluster. As a recent study has shown [11], such interactions and hydrophobic cluster formation play an important role in folding of intrinsically disordered proteins and protein structure stabilization. A number of residues formed this hydrophobic cluster: Val_5, Leu_4, Leu_{19}, Leu_{21}, Val_{34}, Leu_{46} and Tyr_{54} (see Figure S2 in supplementary material). We have found that this region found in the center of PmrD's tertiary structure was completely impermeable from water molecules. The closest distance between any heavy atom of the cluster and oxygen atom of water molecules was 0.45 nm in the MD trajectory. Given the close proximity and strong hydrophobic interactions between these residues (Table 4) it can assumed that the exclusion of water greatly stabilized the protein's 3D structure. Thus, it seems like the driving force for PmrD's folding and stability is again the hydrophobic effect [32].

Time series plot of solvent-accessible surface area (SASA) of the side chain atoms of residues found in the hydrophobic cluster is shown in Fig. 4. The time series averaged around 0.5 nm^2 and showed remarkable stability over simulation time. These data provide clear evidence that solvent remained far from the hydrophobic cluster and β-barrel structure of PmrD benefited a lot from these interactions.

4. Conclusions

Molecular dynamics simulations techniques have been utilized in order to get a clearer view of the 3D structure of PmrD, a protein with a unique β-barrel topology. The simulated structures of PmrD protein offered an opportunity to carefully analyze the non-bonded interactions of the side chains that stabilize the β-barrel structure, something that it is generally hardly achieved by solution NMR

methods, mainly due to high mobility of side chains in aqueous environment. From this point of view, the current study complements the NMR based structural information about the PmrD solution conformation.

Numerous interactions within PmrD's hydrophobic core stabilized the β-barrel structure. The current simulation study revealed an important factor of PmrD's unique fold stability. A hydrophobic cluster, formed by residues of the six strands that consist the protein's β-barrel, were found to be completely impermeable from water molecules. SASA analysis showed that side chains of these residues were very well hidden from solvent interactions. It is ass

Hydrogen bonds between the six β-strands contributed substantially to β-barrel stability. Electrostatic interactions on the surface of PmrD also provide a framework to make some hypotheses about the mode of action or PmrD, mainly around the loops 1 and 2. The Asp_{14}/Arg_{16} pair for example, might play a role on protein/protein interactions, possibly like the RGD motif in cell adhesion processes.

Finally, the current study offers a dynamical view of a novel fold that PmrD protein represents. Models of homologous proteins can be built and studied with molecular dynamics techniques. Moreover, future work with mutated sequence can possibly reveal the individual contribution of key residues to protein stability and protein/protein interaction motifs.

Acknowledgments

We thank the Research Center of Scientific Simulations (RCSS) of University of Ioannina for providing the computational facilities for NAMD parallel execution. We also gratefully acknowledge the open source community for publicly releasing all the computational tools (Linux, NAMD, GNU tools, etc) needed for this research.

Appendix A. Supplementary data

Supplementary data associated with this article can be found, in the online version, at doi:10.1016/j.ijbiomac.2009.02.006.

References

[1] A. Clausell, F. Rabanal, M. Garcia-Subirats, M. Asuncion Alsina, Y. Cajal, Luminescence 20 (2005) 117–123.
[2] D. Landman, C. Georgescu, D.A. Martin, J. Quale, Clin. Microbiol. Rev. 21 (2008) 449–465.
[3] A.Y. Mitrophanov, E.A. Groisman, Genes Dev. 2 (2008) 2601–2611.
[4] I. Zwir, D. Shin, A. Kato, K. Nishino, T. Latifi, F. Solomon, J.M. Hare, H. Huang, E.A. Groisman, PNAS USA (2005) 2862–2867.
[5] A. Kato, T. Latifi, E.A. Groisman, PNAS USA 100 (2003) 4706–4711.
[6] W. Fu, F. Yang, X. Kang, X. Zhang, Y. Li, B. Xia, C. Jin, Biochem. Biophys. Res. Commun. 361 (2007) 1033–1037.
[7] M. Karplus, J.A. McCammon, Nat. Struct. Biol. 9 (2002) 646–652.
[8] W.F. van Gunsteren, J. Dolenc, A.E. Mark, Curr. Opin. Struct. Biol. 18 (2008) 149–153.
[9] F. Mehrnejad, H. Naderi-Manesh, B. Ranjbar, Proteins 67 (2007) 931–940.
[10] A. Stavrakoudis, I.G. Tsoulos, Z.O. Shenkarev, T.V. Ovchinnikova, Biopolym. Peptide Sci. (2009), doi:10.1002/bip.21149.
[11] L.M. Espinoza-Fonseca, FEBS Lett. 583 (2009) 556–560.
[12] W. Humphrey, A. Dalke, K. Schulten, J. Mol. Graph. 14 (1996) 33–38.
[13] W.L. Jorgensen, J. Chandrasekhar, J.D. Madura, R.W. Impey, M.L. Klein, J. Chem. Phys. 79 (1983) 926–935.
[14] W. Weber, P.H. Hünenberger, J.A. McCammon, J. Phys. Chem. B 104 (2000) 3668–3675.
[15] J.C. Phillips, R. Braun, W. Wang, J. Gumbart, E. Tajkhorshid, E. Villa, C. Chipot, R.D. Skeel, L. Kale, K. Schulten, J. Comput. Chem. 26 (2005) 1781–1802.
[16] A.D. MacKerell, D. Bashford, M. Bellott, R.L. Dunbrack, J.D. Evanseck, M.J. Field, S. Fischer, J. Gao, H. Guo, S. Ha, D. Joseph-McCarthy, L. Kuchnir, K. Kuczera, F.T.K. Lau, C. Mattos, S. Michnick, T. Ngo, D.T. Nguyen, B. Prodhom, W.E. Reiher, B. Roux, M. Schlenkrich, J.C. Smith, R. Stote, J. Straub, M. Watanabe, J. Wiorkiewicz-Kuczera, D. Yin, M. Karplus, J. Phys. Chem. B 102 (1998) 3586–3616.
[17] T. Darden, D. York, L. Pedersen, J. Chem. Phys. 98 (1993) 10089–10092.
[18] J.P. Ryckaert, G. Ciccotti, H.J.C. Berendsen, J. Comput. Phys. 23 (1977) 327–341.
[19] S.E. Feller, Y.H. Zhang, R.W. Pastor, B.R. Brooks, J. Chem. Phys. 103 (1995) 4613–4621.
[20] N.M. Glykos, J. Comput. Chem. 27 (2006) 1765–1768.
[21] I.G. Tsoulos, A. Stavrakoudis, Eucb: A C++ Program for Trajectory Analysis, 2009, http://stavrakoudis.econ.uoi.gr/eucb.
[22] D. Frishman, P. Argos, Proteins 23 (1995) 566–579.
[23] W. Delano, The PYMOL Molecular Graphics System, Delano Scientific, San Carlos, CA, 2002.
[24] S.J. Hubbard, J.M. Thornton, NACCESS, Department of Biochemistry and Molecular Biology, University College London, 1993.
[25] A. Stavrakoudis, Chem. Phys. Lett. 461 (2008) 294–299.
[26] Alexander D. Mackerell Jr., Michael Feig, Charles L. Brooks III, J. Comput. Chem. 25 (2004) 1400–1415.
[27] T. Xiao, J. Takagi, B.S. Coller, J.H. Wang, T.A. Springer, Nature 432 (2004) 59–67.
[28] A. Stavrakoudis, G. Bizos, D. Eleftheriadis, A. Kouki, E. Panou-Pomonis, M. Sakarellos-Daitsiotis, C. Sakarellos, D. Tsoukatos, V. Tsikaris, Biopolymers 56 (2001) 20–26.
[29] N. Biris, A. Stavrakoudis, A.S. Politou, E. Mikros, M. Sakarellos-Daitsiotis, C. Sakarellos, V. Tsikaris, Biopolymers 69 (2003) 72–86.
[30] S. Kostidis, A. Stavrakoudis, N. Biris, D. Tsoukatos, C. Sakarellos, V. Tsikaris, J. Pept. Sci. 10 (2004) 494–509.
[31] A. Stavrakoudis, V. Tsikaris, J. Pept. Sci. 14 (2008) 1259–1270.
[32] D. Chandler, Nature 437 (2005) 640–647.

Supplementary Material: Insights into the structure of the PmrD protein with molecular dynamics simulations

Vasileios A. Tatsis, Ioannis G. Tsoulos, Christos S Krinas, Charalampos Alexopoulos and Athanassios Stavrakoudis

Table S1: Average Distances calculated from MD (3rd column) and taken from NMR (2nd column) between atom pairs of H^{α} and H^{N} (1st column).

Atom Pair	**UPL**	**Average Distance MD**
Cys_{10}:H^{N}–Cys_{9}:H^{N}	0.500	0.425
Asn_{11}:H^{α}–Asp_{14}:H^{N}	0.500	0.535
Lys_{12}:H^{N}–Asn_{11}:H^{α}	0.360	0.236
Lys_{12}:H^{N}–Gln_{13}:H^{N}	0.360	0.250
Lys_{12}:H^{α}–Asn_{15}:H^{N}	0.360	0.595
Lys_{12}:H^{α}–Asn_{15}:H^{α}	0.500	0.569
Gln_{13}:H^{N}–Lys_{12}:H^{α}	0.360	0.358
Gln_{13}:H^{N}–Asp_{14}:H^{N}	0.360	0.250
Gln_{13}:H^{α}–Asp_{14}:H^{N}	0.360	0.358
Asp_{14}:H^{N}–Asn_{15}:H^{N}	0.280	0.326
Asp_{14}:H^{α}–Asn_{15}:H^{N}	0.360	0.250
Asp_{14}:H^{α}–Arg_{16}:H^{N}	0.500	0.458
Asn_{15}:H^{N}–Gln_{13}:H^{α}	0.500	0.574
Asn_{15}:H^{N}–Arg_{16}:H^{N}	0.280	0.272
Asn_{15}:H^{α}–Asp_{14}:H^{N}	0.500	0.513
Asn_{15}:H^{α}–Arg_{16}:H^{N}	0.360	0.256
Arg_{16}:H^{N}–His_{17}:H^{N}	0.500	0.435
Arg_{16}:H^{N}–Ala_{84}:H^{α}	0.500	0.705
Arg_{16}:H^{α}–His_{17}:H^{N}	0.280	0.228
His_{17}:H^{N}–Val_{18}:H^{N}	0.500	0.446
His_{17}:H^{α}–Val_{18}:H^{N}	0.280	0.226
Val_{18}:H^{N}–Cys_{9}:H^{N}	0.500	0.297
Val_{18}:H^{α}–Leu_{19}:H^{N}	0.280	0.217
Val_{18}:H^{α}–Glu_{33}:H^{N}	0.500	0.481
Val_{18}:H^{α}–Glu_{33}:H^{α}	0.280	0.241
Leu_{19}:H^{N}–Val_{18}:H^{N}	0.500	0.427
Leu_{19}:H^{N}–Met_{20}:H^{N}	0.500	0.448
Leu_{19}:H^{N}–Glu_{33}:H^{α}	0.360	0.338
Leu_{19}:H^{N}–Val_{34}:H^{N}	0.500	0.410

Atom Pair	UPL	Average Distance MD
Leu_{19}:H^{α}–Met_{20}:H^{N}	0.280	0.220
Met_{1}:H^{α}–Glu_{2}:H^{N}	0.280	0.000
Met_{20}:H^{N}–Lys_{7}:H^{N}	0.360	0.290
Met_{20}:H^{N}–Ser_{8}:H^{α}	0.500	0.338
Met_{20}:H^{α}–Leu_{21}:H^{N}	0.280	0.218
Leu_{21}:H^{N}–Ile_{31}:H^{α}	0.500	0.325
Leu_{21}:H^{α}–Cys_{22}:H^{N}	0.280	0.217
Leu_{21}:H^{α}–Leu_{4}:H^{N}	0.500	0.439
Leu_{21}:H^{α}–Val_{5}:H^{α}	0.360	0.289
Leu_{21}:H^{α}–Lys_{6}:H^{N}	0.500	0.293
Cys_{22}:H^{N}–Trp_{3}:H^{α}	0.500	0.446
Cys_{22}:H^{N}–Leu_{4}:H^{N}	0.360	0.297
Cys_{22}:H^{α}–Asp_{23}:H^{N}	0.280	0.250
Cys_{22}:H^{α}–Lys_{29}:H^{α}	0.360	0.260
Cys_{22}:H^{α}–Met_{30}:H^{N}	0.500	0.377
Asp_{23}:H^{N}–Ile_{28}:H^{N}	0.500	0.384
Asp_{23}:H^{α}–Ala_{24}:H^{N}	0.280	0.273
Asp_{23}:H^{α}–Gly_{25}:H^{N}	0.500	0.470
Asp_{23}:H^{α}–Trp_{3}:H^{α}	0.360	0.270
Asp_{23}:H^{α}–Leu_{4}:H^{N}	0.500	0.316
Ala_{24}:H^{N}–Gly_{25}:H^{N}	0.500	0.250
Ala_{24}:H^{N}–Glu_{2}:H^{N}	0.500	0.499
Ala_{24}:H^{α}–Gly_{25}:H^{N}	0.360	0.345
Ala_{24}:H^{α}–Gly_{26}:H^{N}	0.500	0.523
Gly_{25}:H^{N}–Gly_{26}:H^{N}	0.280	0.238
Gly_{25}:H^{N}–Ala_{27}:H^{N}	0.500	0.410
Gly_{26}:H^{N}–Ala_{27}:H^{N}	0.360	0.224
Ala_{27}:H^{N}–Ile_{28}:H^{N}	0.280	0.251
Ala_{27}:H^{α}–Ile_{28}:H^{N}	0.360	0.347
Ile_{28}:H^{N}–Lys_{29}:H^{N}	0.500	0.446
Ile_{28}:H^{α}–Lys_{29}:H^{N}	0.280	0.226
Lys_{29}:H^{N}–Met_{30}:H^{N}	0.500	0.446
Lys_{29}:H^{α}–Asp_{23}:H^{N}	0.500	0.435
Lys_{29}:H^{α}–Met_{30}:H^{N}	0.280	0.230
Glu_{2}:H^{N}–Trp_{3}:H^{N}	0.500	0.444
Glu_{2}:H^{α}–Met_{1}:H^{α}	0.500	0.443
Glu_{2}:H^{α}–Trp_{3}:H^{N}	0.280	0.223
Glu_{2}:H^{α}–Leu_{46}:H^{N}	0.500	0.488

Atom Pair	UPL	Average Distance MD
Glu_{2}:H^{α}–Ser_{47}:H^{α}	0.500	0.291
Met_{30}:H^{α}–Ile_{31}:H^{N}	0.280	0.233
Met_{30}:H^{α}–Ser_{71}:H^{N}	0.500	0.544
Met_{30}:H^{α}–Ser_{71}:H^{α}	0.360	0.291
Met_{30}:H^{α}–Tyr_{72}:H^{N}	0.280	0.320
Ile_{31}:H^{N}–Ser_{71}:H^{α}	0.500	0.364
Ile_{31}:H^{α}–Ala_{32}:H^{N}	0.280	0.223
Ala_{32}:H^{N}–Met_{20}:H^{α}	0.500	0.376
Ala_{32}:H^{N}–Glu_{33}:H^{N}	0.500	0.432
Ala_{32}:H^{α}–Ile_{31}:H^{N}	0.500	0.485
Ala_{32}:H^{α}–Glu_{33}:H^{N}	0.280	0.218
Glu_{33}:H^{N}–Val_{34}:H^{N}	0.500	0.438
Glu_{33}:H^{N}–Ser_{68}:H^{N}	0.360	0.319
Glu_{33}:H^{N}–Ala_{69}:H^{α}	0.500	0.333
Glu_{33}:H^{α}–Val_{34}:H^{N}	0.280	0.220
Glu_{33}:H^{α}–Val_{34}:H^{α}	0.500	0.442
Val_{34}:H^{N}–Val_{18}:H^{α}	0.360	0.351
Val_{34}:H^{α}–Lys_{35}:H^{N}	0.280	0.225
Val_{34}:H^{α}–Val_{66}:H^{α}	0.360	0.243
Val_{34}:H^{α}–Leu_{67}:H^{N}	0.360	0.257
Lys_{35}:H^{N}–Val_{66}:H^{α}	0.500	0.368
Lys_{35}:H^{N}–Leu_{67}:H^{N}	0.500	0.400
Lys_{35}:H^{α}–Ser_{36}:H^{N}	0.280	0.222
Ser_{36}:H^{N}–Asp_{37}:H^{N}	0.500	0.411
Asp_{37}:H^{N}–Phe_{38}:H^{N}	0.360	0.230
Asp_{37}:H^{α}–Phe_{38}:H^{N}	0.360	0.357
Phe_{38}:H^{N}–Ala_{39}:H^{N}	0.500	0.406
Phe_{38}:H^{α}–Asp_{37}:H^{N}	0.500	0.486
Phe_{38}:H^{α}–Ala_{39}:H^{N}	0.280	0.245
Ala_{39}:H^{α}–Val_{40}:H^{N}	0.280	0.224
Trp_{3}:H^{N}–Leu_{46}:H^{N}	0.360	0.313
Trp_{3}:H^{N}–Ser_{47}:H^{α}	0.500	0.389
Trp_{3}:H^{α}–Ala_{24}:H^{N}	0.500	0.462
Trp_{3}:H^{α}–Leu_{4}:H^{N}	0.280	0.221
Val_{40}:H^{N}–Lys_{41}:H^{N}	0.500	0.441
Val_{40}:H^{α}–Lys_{41}:H^{N}	0.280	0.221
Lys_{41}:H^{α}–Val_{42}:H^{N}	0.280	0.245
Lys_{41}:H^{α}–Ser_{8}:H^{N}	0.500	0.661

Atom Pair	UPL	Average Distance MD
Val_{42}:H^N–Lys_{41}:H^N	0.500	0.450
Val_{42}:H^N–Gly_{43}:H^N	0.500	0.454
Val_{42}:H^α–Gly_{43}:H^N	0.280	0.221
Val_{42}:H^α–Asp_{44}:H^N	0.360	0.342
Val_{42}:H^α–Lys_{7}:H^α	0.500	0.484
Gly_{43}:H^N–Asp_{44}:H^N	0.280	0.255
Asp_{44}:H^N–Leu_{45}:H^N	0.500	0.458
Asp_{44}:H^N–Val_{5}:H^N	0.500	0.388
Asp_{44}:H^α–Leu_{45}:H^N	0.280	0.231
Asp_{44}:H^α–Val_{5}:H^N	0.500	0.497
Leu_{45}:H^N–Leu_{46}:H^N	0.500	0.445
Leu_{45}:H^N–Asn_{57}:H^N	0.360	0.338
Leu_{45}:H^N–Asn_{57}:H^α	0.360	0.343
Leu_{45}:H^α–Trp_{3}:H^N	0.500	0.472
Leu_{45}:H^α–Leu_{46}:H^N	0.280	0.220
Leu_{45}:H^α–Leu_{4}:H^α	0.280	0.247
Leu_{45}:H^α–Val_{5}:H^N	0.360	0.340
Leu_{46}:H^N–Leu_{4}:H^α	0.500	0.349
Leu_{46}:H^N–Val_{5}:H^N	0.500	0.433
Leu_{46}:H^α–Ser_{47}:H^N	0.280	0.215
Leu_{46}:H^α–Cys_{55}:H^N	0.500	0.425
Leu_{46}:H^α–Ile_{56}:H^α	0.500	0.285
Leu_{46}:H^α–Asn_{57}:H^N	0.500	0.339
Ser_{47}:H^N–Leu_{46}:H^N	0.500	0.427
Ser_{47}:H^N–Cys_{55}:H^N	0.360	0.300
Pro_{48}:H^α–Leu_{49}:H^N	0.280	0.223
Pro_{48}:H^α–Gln_{50}:H^N	0.500	0.428
Pro_{48}:H^α–Tyr_{54}:H^α	0.280	0.247
Leu_{49}:H^N–Gln_{50}:H^N	0.360	0.231
Leu_{49}:H^N–Gln_{50}:H^α	0.500	0.460
Leu_{49}:H^N–Tyr_{54}:H^α	0.360	0.229
Leu_{49}:H^N–Cys_{55}:H^N	0.500	0.384
Leu_{49}:H^α–Pro_{48}:H^α	0.500	0.445
Leu_{49}:H^α–Gln_{50}:H^N	0.500	0.358
Leu_{4}:H^N–Trp_{3}:H^N	0.500	0.447
Leu_{4}:H^N–Val_{5}:H^N	0.500	0.447
Leu_{4}:H^α–Asp_{44}:H^N	0.500	0.552
Leu_{4}:H^α–Leu_{45}:H^N	0.500	0.498

Atom Pair	UPL	Average Distance MD
Leu_{4}:H^{α}–Val_{5}:H^{N}	0.280	0.222
Asn_{51}:H^{N}–Gln_{50}:H^{α}	0.360	0.319
Asn_{51}:H^{N}–Ala_{52}:H^{N}	0.500	0.253
Asn_{51}:H^{α}–Gln_{50}:H^{N}	0.500	0.491
Asn_{51}:H^{α}–Ala_{52}:H^{N}	0.360	0.359
Ala_{52}:H^{N}–Leu_{53}:H^{N}	0.360	0.229
Ala_{52}:H^{α}–Leu_{53}:H^{N}	0.360	0.347
Ala_{52}:H^{α}–Val_{66}:H^{N}	0.500	0.372
Leu_{53}:H^{N}–Asn_{51}:H^{α}	0.500	0.459
Leu_{53}:H^{N}–Tyr_{54}:H^{N}	0.500	0.444
Leu_{53}:H^{N}–Lys_{65}:H^{α}	0.500	0.469
Leu_{53}:H^{α}–Tyr_{54}:H^{N}	0.280	0.214
Tyr_{54}:H^{N}–Cys_{55}:H^{N}	0.500	0.446
Tyr_{54}:H^{α}–Gln_{50}:H^{N}	0.500	0.385
Tyr_{54}:H^{α}–Cys_{55}:H^{N}	0.280	0.244
Cys_{55}:H^{N}–Pro_{48}:H^{α}	0.500	0.374
Cys_{55}:H^{N}–Ile_{56}:H^{N}	0.500	0.445
Cys_{55}:H^{α}–Ile_{56}:H^{N}	0.280	0.233
Cys_{55}:H^{α}–Ile_{56}:H^{α}	0.500	0.430
Cys_{55}:H^{α}–Lys_{60}:H^{α}	0.500	0.479
Cys_{55}:H^{α}–Thr_{63}:H^{α}	0.280	0.225
Cys_{55}:H^{α}–Val_{64}:H^{N}	0.500	0.305
Ile_{56}:H^{N}–Thr_{63}:H^{α}	0.500	0.356
Ile_{56}:H^{α}–Ser_{47}:H^{N}	0.500	0.351
Ile_{56}:H^{α}–Asn_{57}:H^{N}	0.280	0.213
Asn_{57}:H^{N}–Ile_{56}:H^{N}	0.500	0.445
Asn_{57}:H^{N}–Arg_{58}:H^{N}	0.500	0.443
Asn_{57}:H^{N}–Glu_{59}:H^{N}	0.500	0.619
Asn_{57}:H^{α}–Arg_{58}:H^{N}	0.360	0.342
Asn_{57}:H^{α}–Arg_{58}:H^{α}	0.500	0.438
Arg_{58}:H^{N}–Glu_{59}:H^{N}	0.360	0.231
Arg_{58}:H^{α}–Glu_{59}:H^{N}	0.360	0.360
Glu_{59}:H^{N}–Lys_{60}:H^{N}	0.500	0.460
Glu_{59}:H^{N}–Lys_{60}:H^{α}	0.500	0.547
Glu_{59}:H^{α}–Lys_{60}:H^{N}	0.280	0.230
Glu_{59}:H^{α}–Lys_{60}:H^{α}	0.500	0.432
Glu_{59}:H^{α}–Leu_{61}:H^{N}	0.500	0.429
Val_{5}:H^{N}–Gly_{43}:H^{N}	0.500	0.378

Atom Pair	UPL	Average Distance MD
Val_5:H^{α}–Met_{20}:H^N	0.360	0.475
Val_5:H^{α}–Cys_{22}:H^N	0.500	0.402
Val_5:H^{α}–Leu_4:H^{α}	0.500	0.440
Val_5:H^{α}–Lys_6:H^N	0.280	0.216
Val_5:H^{α}–Lys_7:H^N	0.360	0.410
Lys_{60}:H^{α}–Leu_{61}:H^N	0.360	0.270
Lys_{60}:H^{α}–His_{62}:H^N	0.500	0.439
Leu_{61}:H^{α}–His_{62}:H^N	0.360	0.360
His_{62}:H^N–Glu_{59}:H^N	0.500	0.593
His_{62}:H^N–Thr_{63}:H^N	0.500	0.425
His_{62}:H^{α}–Thr_{63}:H^N	0.280	0.222
Thr_{63}:H^N–Val_{64}:H^N	0.500	0.452
Thr_{63}:H^{α}–Val_{64}:H^N	0.280	0.222
Val_{64}:H^N–Ile_{56}:H^N	0.500	0.475
Val_{64}:H^N–Lys_{65}:H^N	0.500	0.421
Val_{64}:H^{α}–Ser_{36}:H^N	0.500	0.589
Val_{64}:H^{α}–Asp_{37}:H^N	0.360	0.450
Val_{64}:H^{α}–Lys_{65}:H^N	0.280	0.221
Lys_{65}:H^{α}–Ala_{52}:H^{α}	0.500	0.509
Lys_{65}:H^{α}–Val_{66}:H^N	0.280	0.218
Lys_{65}:H^{α}–Val_{66}:H^{α}	0.500	0.442
Val_{66}:H^N–Ala_{52}:H^N	0.500	0.575
Val_{66}:H^{α}–Leu_{67}:H^N	0.280	0.217
Val_{66}:H^{α}–Ser_{68}:H^N	0.500	0.440
Leu_{67}:H^N–Ser_{68}:H^N	0.280	0.257
Leu_{67}:H^{α}–Ser_{68}:H^N	0.360	0.355
Ser_{68}:H^N–Val_{34}:H^{α}	0.500	0.467
Ser_{68}:H^{α}–Glu_{33}:H^N	0.500	0.491
Ser_{68}:H^{α}–Ala_{69}:H^N	0.280	0.224
Ala_{69}:H^N–Ser_{70}:H^N	0.500	0.439
Ala_{69}:H^{α}–Ser_{68}:H^N	0.500	0.484
Ala_{69}:H^{α}–Ser_{68}:H^{α}	0.500	0.443
Ala_{69}:H^{α}–Ser_{70}:H^N	0.280	0.227
Lys_6:H^N–Met_{20}:H^N	0.360	0.411
Lys_6:H^N–Val_5:H^N	0.500	0.440
Lys_6:H^N–Lys_7:H^N	0.280	0.245
Ser_{70}:H^N–Ala_{32}:H^{α}	0.360	0.350
Ser_{70}:H^N–Ser_{71}:H^N	0.500	0.436

Atom Pair	UPL	Average Distance MD
Ser_{70}:H^{α}–Ala_{69}:H^{N}	0.500	0.496
Ser_{71}:H^{N}–Tyr_{72}:H^{N}	0.500	0.459
Ser_{71}:H^{α}–Tyr_{72}:H^{N}	0.280	0.240
Tyr_{72}:H^{N}–Ile_{31}:H^{N}	0.500	0.450
Tyr_{72}:H^{N}–Ser_{73}:H^{N}	0.500	0.436
Ser_{73}:H^{N}–Tyr_{72}:H^{α}	0.280	0.215
Ser_{73}:H^{N}–Glu_{76}:H^{N}	0.500	0.408
Ser_{73}:H^{N}–Trp_{77}:H^{N}	0.500	0.386
Pro_{74}:H^{α}–Asp_{75}:H^{N}	0.360	0.346
Asp_{75}:H^{N}–Ser_{73}:H^{α}	0.500	0.389
Asp_{75}:H^{N}–Glu_{76}:H^{N}	0.280	0.255
Asp_{75}:H^{α}–Glu_{76}:H^{N}	0.500	0.356
Asp_{75}:H^{α}–Glu_{78}:H^{N}	0.360	0.360
Asp_{75}:H^{α}–Arg_{79}:H^{N}	0.500	0.405
Glu_{76}:H^{N}–Trp_{77}:H^{N}	0.360	0.273
Glu_{76}:H^{N}–Glu_{78}:H^{N}	0.500	0.435
Glu_{76}:H^{α}–Glu_{78}:H^{N}	0.500	0.464
Glu_{76}:H^{α}–Arg_{79}:H^{N}	0.360	0.352
Glu_{76}:H^{α}–Gln_{80}:H^{N}	0.360	0.405
Trp_{77}:H^{N}–Pro_{74}:H^{α}	0.500	0.337
Trp_{77}:H^{N}–Glu_{78}:H^{N}	0.360	0.282
Glu_{78}:H^{N}–Trp_{77}:H^{α}	0.500	0.360
Glu_{78}:H^{α}–Cys_{81}:H^{N}	0.500	0.342
Arg_{79}:H^{N}–Gln_{80}:H^{N}	0.360	0.283
Lys_{7}:H^{N}–Leu_{19}:H^{α}	0.500	0.466
Lys_{7}:H^{N}–Ser_{8}:H^{N}	0.500	0.437
Lys_{7}:H^{α}–Val_{42}:H^{N}	0.500	0.604
Lys_{7}:H^{α}–Ser_{8}:H^{N}	0.280	0.234
Gln_{80}:H^{N}–Arg_{79}:H^{α}	0.500	0.359
Gln_{80}:H^{N}–Cys_{81}:H^{N}	0.360	0.272
Gln_{80}:H^{N}–Lys_{82}:H^{N}	0.500	0.427
Gln_{80}:H^{α}–Cys_{81}:H^{N}	0.280	0.357
Cys_{81}:H^{N}–Arg_{79}:H^{α}	0.500	0.454
Cys_{81}:H^{N}–Lys_{82}:H^{N}	0.280	0.277
Lys_{82}:H^{N}–Glu_{78}:H^{α}	0.500	0.401
Lys_{82}:H^{N}–Arg_{79}:H^{α}	0.500	0.356
Lys_{82}:H^{N}–Gln_{80}:H^{α}	0.500	0.437
Lys_{82}:H^{N}–Cys_{81}:H^{α}	0.500	0.357

Atom Pair	UPL	Average Distance MD
Lys_{82}:H^N–Val_{83}:H^N	0.360	0.272
Lys_{82}:H^α–Val_{83}:H^N	0.360	0.355
Val_{83}:H^N–Gln_{80}:H^α	0.500	0.345
Val_{83}:H^N–Ala_{84}:H^N	0.360	0.260
Val_{83}:H^α–Lys_{82}:H^N	0.500	0.533
Val_{83}:H^α–Ala_{84}:H^N	0.360	0.357
Ala_{84}:H^N–Cys_{81}:H^α	0.500	0.335
Ala_{84}:H^α–Gly_{85}:H^N	0.360	0.357
Gly_{85}:H^N–Val_{83}:H^N	0.500	0.445
Lys_{86}:H^N–Val_{83}:H^N	0.500	0.613
Lys_{86}:H^N–Thr_{87}:H^N	0.500	0.264
Lys_{86}:H^α–Gly_{85}:H^N	0.500	0.447
Lys_{86}:H^α–Thr_{87}:H^N	0.280	0.356
Thr_{87}:H^α–Lys_{86}:H^N	0.500	0.509
Thr_{87}:H^α–Gln_{88}:H^N	0.360	0.251
Gln_{88}:H^N–Lys_{82}:H^α	0.500	0.650
Gln_{88}:H^α–Thr_{87}:H^N	0.500	0.504
Ser_8:H^α–Lys_7:H^N	0.500	0.474
Ser_8:H^α–Cys_9:H^N	0.280	0.225
Cys_9:H^N–Ser_8:H^N	0.500	0.430
Cys_9:H^α–Ser_8:H^N	0.500	0.485

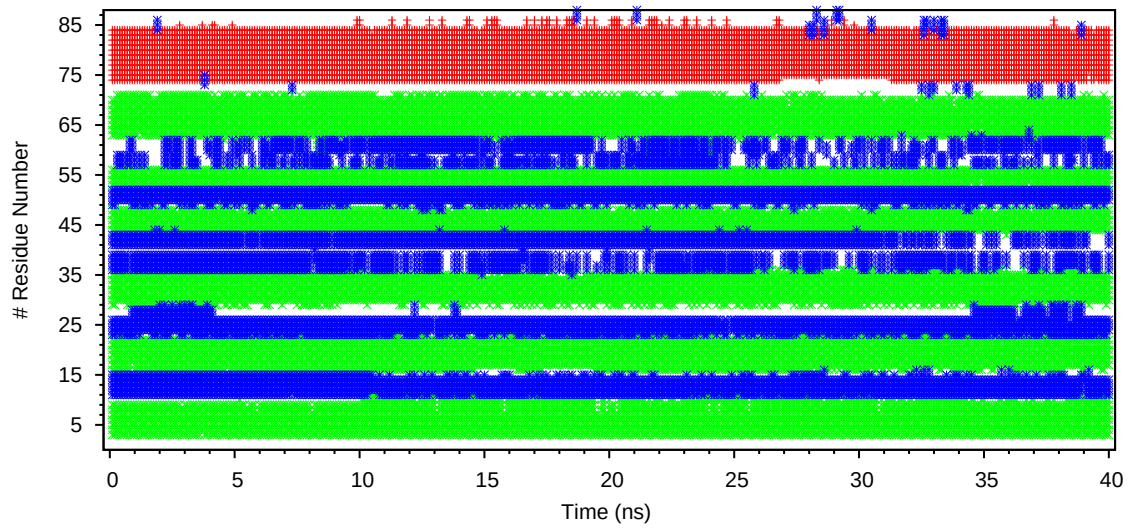

Figure S1: Time evolution of secondary structure assignment (STRIDE). Red, green and blue colors represent helical, strand (extented) and turn conformational assignment respectively.

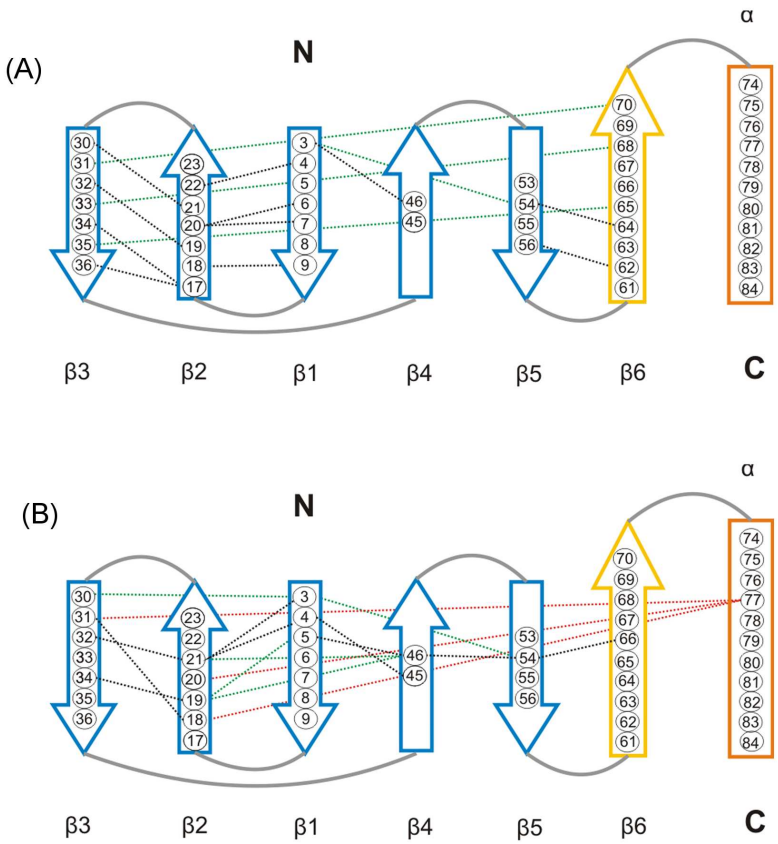

Figure S2. (A) Hydrogen bonds and (B) hydrophobic interactions formed between the residures of E. coli PmrD. The black lines represent interactions between residues that belong to vicinal strands, interactions between residues of non contiguous strands are identified by green lines. The lines that depict the interactions between the residues of the α-helix and the rest of the protein are colored red. Also, the α-helix is colored in red, loops in grey, and β-strands (β1–β5) in cyan, β6 in yellow.

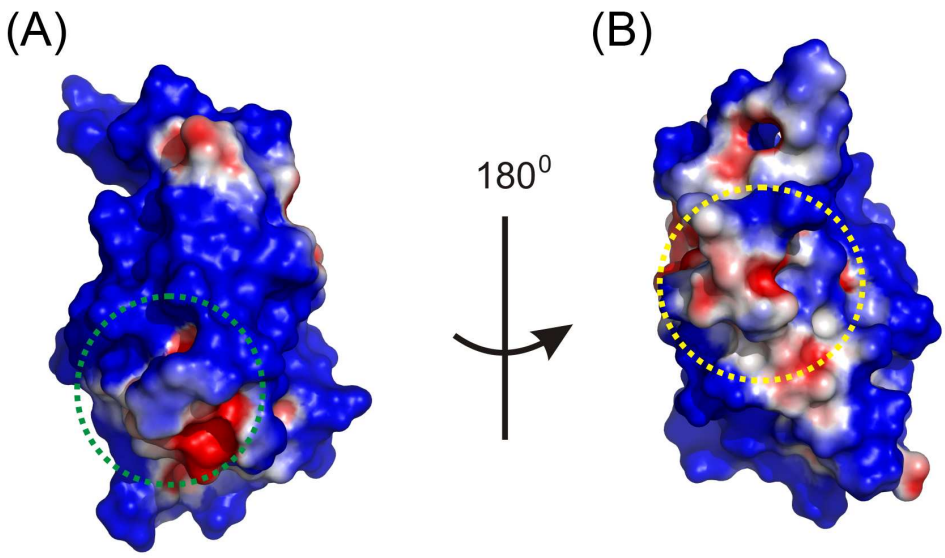

Figure S3.The surface electrostatic potential representations of the E. coli PmrD. The two electropositive regions of PmrD are indicated by dashed circles (the region around loop 1 in yellow, region around loop 2 in green) in (A) and (B).